Nonuniformly Driven Two-Plasmon-Decay Instability in Direct-Drive Implosions

W. Seka,* J. F. Myatt, R. W. Short, D. H. Froula, J. Katz, V. N. Goncharov, and I. V. Igumenshchev
Laboratory for Laser Energetics, University of Rochester, 250 East River Road, Rochester, New York 14623-1299, USA
(Received 6 December 2013; published 7 April 2014)

Half-harmonic emission spectra and images taken during directly driven implosions show that the two-plasmon decay (TPD) instability is driven nonuniformly over the target surface and that multibeam effects dominate this instability. The images show a spatially limited extent of the TPD instability. A prominent spectral feature is used to determine the electron temperature in the corona. Near threshold the temperatures agree with one-dimensional hydrodynamic predictions but exceed them by ~10% above the TPD threshold. Two-dimensional hydrodynamic simulations indicate that a significant part (~20%) of the laser intensity must be locally absorbed by the TPD instability (i.e., by collisional damping of the electron plasma waves) to maintain these temperature islands.

DOI: 10.1103/PhysRevLett.112.145001 PACS numbers: 52.50.Jm, 52.35.-g, 52.38.-r

This Letter presents half-integer harmonic images, time-resolved spectra, and time-resolved coronal electron temperatures that show for the first time that the two-plasmon decay (TPD) instability is localized in specific areas of the target surface of laser-driven implosions. These data confirm the multibeam nature of this instability. The nonuniform distribution of this instability is important as it may influence the drive uniformity as well as extrapolations to alternative target configurations.

The two-plasmon-decay (TPD) instability is the decay of an incident laser photon into two plasmons [1–7] that can generate energetic electrons. These energetic electrons can preheat inertial confinement fusion (ICF) [8,9] implosions, degrading their performance.

The phase-matching conditions for the TPD instability restrict it to electron densities of $n_e \lesssim n_c/4$, where n_c is the density where the plasma frequency equals the laser frequency. A lower density limit is imposed by Landau damping [10], where $k_{\max}\lambda_{De} \sim 0.25$ ($k_{\max}$ is the largest TPD wave number and λ_{De} the Debye length). The TPD instability growth rate is maximized for decays whose wave vectors lie on the hyperbola defined by $k_{1_\parallel}(k_{1_\parallel} - k_0) = k_{1_\perp}^2$, where $k_{1_\parallel}$ and $k_{1_\perp}$ are the components of the k vector of the larger of the two TPD plasmons parallel and perpendicular to k_0, and k_0 and ω_0 are the k vector and frequency of the incident photon. The frequencies of the corresponding plasma waves are $\omega_{1,2} = \omega_0/2 \pm \Delta\omega$, where $\Delta\omega/\omega_0 = 4.4 \times 10^{-3}(\vec{k}_1 \bullet \vec{k}_0/k_0^2 - \frac{1}{2})T_{e,keV}$ [11,12]. The smallest frequency shift is obtained when $\vec{k}_1 \approx \vec{k}_2$ and $\Delta\omega/\omega_0$ depends only on T_e. For the present experiments the Landau cutoff lies near $n_e \sim n_c/5$ and $k_1 \sim 3k_0$ resulting frequency shifts that are 2 to 3 times larger than the minimum shifts and depends on both k_1 and T_e.

The TPD instability has been investigated extensively theoretically [1–7,13–22]. For single-beam TPD it was found that the absolute instability near $n_c/4$ has the lowest threshold [6]. For current 351-nm interaction experiments this threshold can be defined as $\eta = 1$, where $\eta \simeq I_{14}L_{n,\mu m}/(233\,T_{e,keV})$ and I_{14}, L_n, and T_e are the intensity, density scale length, and electron temperature at $n_c/4$ in units of 10^{14} W/cm^2, μm, and keV, respectively. Two-dimensional extended Zakharov simulations [20,21] that include kinetic effects (quasilinear diffusion model) have shown that two incident EM waves can also effectively drive the TPD instability with thresholds determined by the overlapped intensity provided the polarization of the incident beams is in the plane of the simulations. A three-dimensional extension [22] of these simulations has further shown that for beams with the same polar angle, θ, relative to the target normal, the absolute TPD threshold, in most cases, is still well approximated by the Simon formula ($\eta = 1$) provided I_{14} is replaced with the sum of local beam intensities at $n_c/4$. These results are further supported by a theoretical multibeam TPD analysis [23] that follows an approach analogous to the original absolute TPD instability analysis [6].

The TPD instability is generally accompanied by optical emission near $\omega_0/2$ and $3\omega_0/2$. These spectra loosely reflect the frequencies of the TPD plasma waves. A sharp redshifted feature seen in the $\omega/2$ spectra is due to long wavelength decays, probably associated with the absolute TPD instability [6] near $n_c/4$ and arises most likely from inverse resonance absorption [12,24,25] that converts the lower-frequency TPD plasmons to photons, both of whose wave numbers nearly vanish. This spectral feature can only be observed along the direction of the density gradient. It provides a powerful electron-temperature diagnostic [12] close to the $n_c/4$ surface ($T_{e,keV} \approx \Delta\lambda_{nm}/3.1$ for $\lambda_0 = 351$ nm).

Direct-drive planar interaction experiments and spherical implosion experiments demonstrated in 2003 that the TPD instability was a multibeam instability [26]. At that time no theory existed that could explain the multibeam interaction, energetic electron generation, or the different temporal

onsets for the half-integer harmonic radiation and hard x-ray emission. The spectral shifts and widths of the $\omega/2$ and $3\omega/2$ emission indicated that this instability extended well into the low-density regime where TPD is expected to be convective on the basis of linear theory [11,12]. Recent work has shown the effect of beam configurations, polarization, and intensity on the scaling of hot-electron production resulting from TPD [27,28] based on experiments and comparison with linear gain calculations for convectively unstable TPD.

The experiments were carried out on LLE's 60-beam ($\lambda_0 = 351$ nm) OMEGA Laser System [29] using spherical targets. Each beam illuminates the entire hemisphere of the target using distributed phase plates (DPPs) [30] and smoothing by spectral dispersion (SSD) [31]. (Past experience has shown that this instability is insensitive to SSD [11]. Sensitivity to polarization smoothing is expected but has not been investigated experimentally.) Time-resolved $\omega/2$ spectra were recorded in three locations: one through a beam port and two through diagnostic ports (hex or pent ports) centered on five or six symmetrically located beams at $\theta \approx 23°$ (see Fig. 1). The signals from beam and hex ports were collected and relayed by optical fibers to a time-multiplexed, 1/3-m spectrometer. The signal from the pent port was optically relayed to a similar spectrometer. Both spectrometers were proximity coupled to ROSS streak cameras [32]. Typical spectral and temporal resolutions were ~1 nm and ~100 ps, respectively. All streak records were routinely corrected for geometric and sweep-speed nonlinearities to ~1% residual nonlinearity. The two multiplexed spectra viewed the entire target sphere, while the spectra recorded in the pent location viewed an ~50-μm × 50-μm area on the target sphere.

Half-harmonic images were recorded on a charge-coupled-device (CCD) camera at the center of another hex port. Colored glass and interference filters at the camera input passed either the entire $\omega/2$ spectrum (680 and 720 nm) or only the blue part of the spectrum (680 to 700 nm). (The central $\omega_0/2$ wavelength lies at 702 nm.)

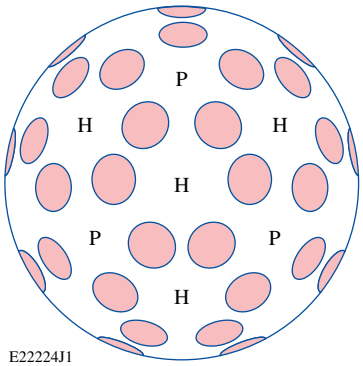

FIG. 1 (color online). Schematic of the OMEGA target chamber with beam ports (shaded) and the locations of hex (H) and pent (P) ports. $\omega/2$ spectra were recorded through one of the beam ports and centered on one of the H and P ports.

Representative $\omega/2$ spectra recorded at the center of the pent port are shown in Fig. 2 for two viewing directions: one viewing an imploding target radially along the density gradient (target normal) [Fig. 2(a)]; the other one displaced by ~100 μm and inclined by ~10° relative to the target normal [Fig. 2(d)]. A schematic of the experimental layout is shown in Fig. 2(c). The sharp redshifted spectral feature dominates in Fig. 2(a) in contrast to Fig. 2(d). At the point of observation (pent port), the absolute TPD intensity threshold lies far above the single-beam intensity ($\eta \sim 0.06$).

The frequency shift in THz, $\Delta\nu$, of the sharp redshifted spectrum in Fig. 2(a) indicates an electron temperature at $n_c/4$ of $T_e \approx 1.66$ keV at t ~ 0.7 ns, in good agreement with one-dimensional hydrodynamic LILAC [33] predictions [green line in Fig. 2(b)]. These predictions include nonlocal electron transport [34] and cross-beam energy transfer [35] and reproduce well most aspects of current LLE implosions.[34] This experiment was close to the experimental TPD threshold and no hard x-ray emission due to energetic electron production was observed.

Figure 2(d) shows the off-axis $\omega/2$ spectrum that is dominated by a broad blue-shifted spectral feature corresponding to TPD decays at densities down to $n_c/5$. To generate this feature requires either Thomson downward scattering (TDS) off TPD plasmons using any of the 60 OMEGA beams as probe beams, and/or inverse parametric decay (IPD) [12,25] in which plasma waves and ion waves of roughly equal wave numbers beat to generate $\omega/2$

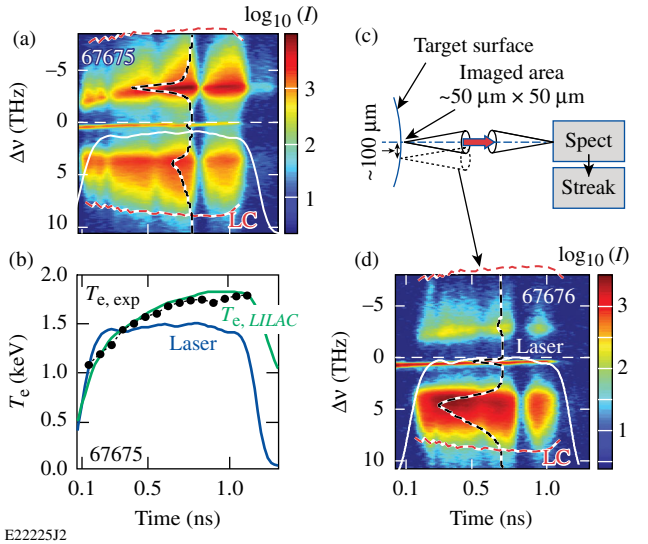

FIG. 2 (color online). Time-resolved $\omega/2$ spectra viewing a small area on the target surface. (a) Spectrum taken along the target normal, (b) inferred electron temperatures (black dots), LILAC predictions (green line), (c) schematic setup for time-resolved $\omega/2$ spectroscopy, (d) equivalent $\omega/2$ spectrum taken ~10° off the target normal. Landau cutoff frequencies are shown as red/white dashed lines in (a) and (d) and are denoted by LC.

photons. Analysis shows that the k-matching conditions for TDS off primary TPD plasma waves on the maximum TPD growth rate curve cannot be fulfilled using any of the OMEGA beams. TDS can account for part of the $\omega/2$ spectrum provided the unstable plasma wave spectrum is broadened within the Landau cutoff limit as predicted by nonlinear Zakharov simulations [20–22]. However, the very small $\omega/2$ photon wave numbers, $k_{\omega/2}/k_0 \lesssim 0.2$ impose severe restrictions on TDS, limiting the spectral range that can be generated to below that observed. To reconcile the observed $\omega/2$ spectra IPD must be invoked. In either case, the broad $\omega/2$ spectra extending all the way to the Landau cutoff (LC in Fig. 2) and their rapid turn-on are indicative of the nonlinear phase of the TPD instability since only the nonlinear phase of the TPD instability can generate the requisite broad plasma wave spectrum.

Images of the $\omega/2$ emission (Fig. 3) provide information regarding the localization and the multibeam nature of the TPD instability. Figure 3(a) was filtered to observe the entire $\omega/2$ spectrum (680 to 740 nm) for an imploding target with maximum overlapped vacuum laser intensity $I_{\max} \sim 10^{15}$ W/cm^2, while in Fig. 3(b) only the blue $\omega/2$ component was recorded (680 to 700 nm). A scale superposed in Fig. 3(a) translates the spatial information in the images into polar angles on the target where the $\omega/2$ emission is generated. Figure 3(c) shows two lineouts through the centers of Figs. 3(a) and 3(b).

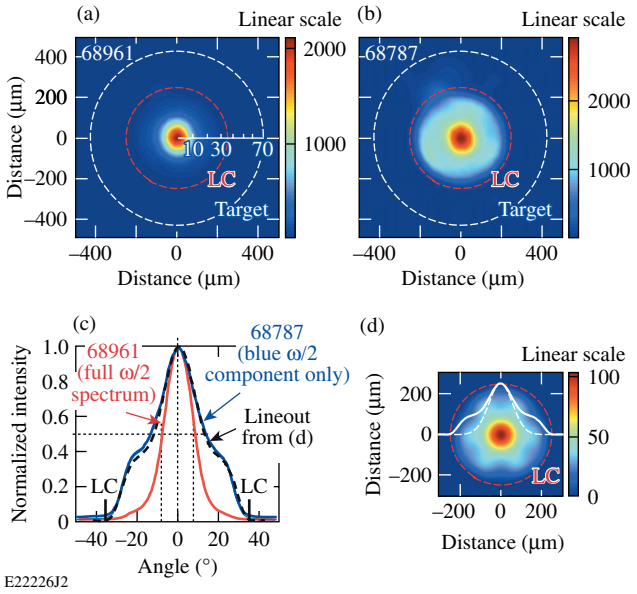

FIG. 3 (color online). $\omega/2$ images taken through a hex port (surrounded by six beams). (a) Image of an imploding target filtered for 680 nm $< \lambda <$ 740 nm, (b) same as in (a) but filtered for 680 nm $< \lambda <$ 700 nm, (c) cross-sectional lineouts through the center of the target for (a), (b), and (d), and (d) simulated $\omega/2$ image using 10° half-angle emission cones at the hex, beam, and neighboring pent ports including a super-Gaussian cutoff to simulate the angular emission limitations due to refraction.

Figure 3(a) is dominated by the sharp red feature in Fig. 2(a). This emission is guided parallel to the density gradient due to refraction. The emission cone angle is determined by $k_\perp/k_{\omega/2} \lesssim 0.1$ for decays at the highest densities. The corresponding calculated emission angle outside the plasma (after refraction) is ~5.5°, close to the measured angle of ~6° after deconvolving the $f/10$ imaging optics from the observed 8° half-cone angle. These planar geometry estimates are valid for rays of near-normal incidence relevant here.

The $\omega/2$ image in Fig. 3(b) does not include the red part of the $\omega/2$ spectrum [see Fig. 2(d)] and is mostly due to $\omega/2$ emission from lower densities corresponding to $\omega/2$ photons with the largest wave numbers. Assuming that these photons can be emitted in any direction, including at 90° to the target normal, i.e., $k_\parallel = 0$, one finds that refraction in the spherical corona changes the emission angle to ~37° outside the plasma. If the $\omega/2$ source were isotropic (Lambertian) over the entire near-quarter-critical surface, the image intensity would smoothly drop to zero at the polar angle $\theta_{\rm LC} \sim 37°$ following Lambert's cosine law as modified by refraction. The $f/10$ imaging optics raises this limit slightly; its location is indicated in Fig. 3 by LC (red dashed circles). There is indeed only scant emission at or beyond the Landau cutoff consistent with past results [12].

The multibeam nature of the TPD instability is evident in Figs. 3(b)–(d). The lineouts show a central emission surrounded by side lobes at ~23°. The side lobes correspond to the locations of the six beams surrounding the hex port. These distinct side lobes indicate TPD instability areas localized at the hex (pent) centers as well as the beam locations rather than being uniformly spread around the entire target sphere. Modeling the image in Fig. 3(b) with super-Gaussian intensity distributions centered on the hex port and the six surrounding beam ports yields Fig. 3(d), which closely resembles Fig. 3(b) including the lineouts. This composite image includes a smooth (super-Gaussian) cutoff at 37°, the Landau cutoff angle for each individual super-Gaussian as well as the entire image. The TPD-affected areas thus identified are 50 to 100 μm in radius for implosions of 860-μm diameter targets. A more accurate estimate of the interaction areas requires detailed knowledge of the nonlinear TPD plasma wave spectrum and a clearer identification of the $\omega/2$ generation process.

For the experimental conditions of Fig. 3, theoretical estimates of the absolute TPD threshold [23] indicate that all beams that cross a particular area on the $n_c/4$ surface can contribute regardless of angle of incidence. This is a consequence of the small-k plasma waves that are shared in this interaction. Including refraction, absorption, cross-beam energy transfer and beam angles, these estimates showed that the calculated TPD threshold increases rapidly near the lowest threshold area, typically located at the hex port centers. This increase occurs within ~5° of the hex port center corresponding to ~50 μm radius on the 860-μm

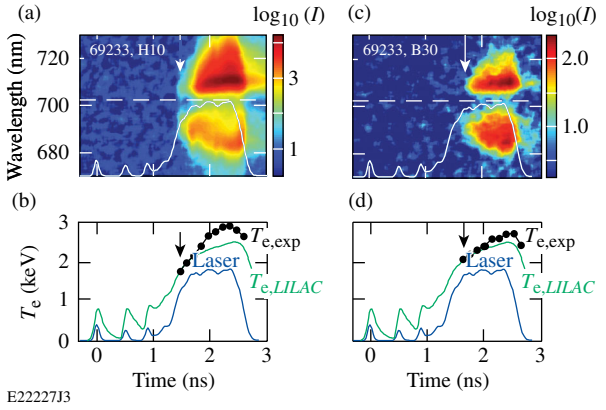

FIG. 4 (color online). $\omega/2$ spectra taken for an imploding room-temperature target at 9.3×10^{14} W/cm^2 through (a) a hex port and (c) a beam port. The laser pulse shape is shown in each panel. The sharp red-shifted features in (a) and (c) were used to measure T_e in (b) and (d). Random error bars are equal to the symbol sizes. Hydrodynamic predictions for T_e are shown in green. Arrows indicate the onset of $\omega/2$ emission and estimated TPD thresholds.

diameter target. These conclusions are in contrast to interactions that share the larger-k plasma waves for which only beams of equal polar angle can contribute [27,28].

Figure 4 shows two $\omega/2$ spectra taken at the centers of a hex and a beam port, respectively. The different onset times of the $\omega/2$ emission are consistent with the expected differences in absolute TPD thresholds considering the total number of overlapped beams, their angles of incidence and their intensities including absorption, refraction and cross-beam energy transfer.

At the onset of $\omega/2$ emission in Fig. 4, the measured electron temperatures are very close to one-dimensional hydrodynamic LILAC predictions. As time progresses, the measured temperatures exceed the LILAC predictions significantly. (LILAC does not contain a TPD model or *ad hoc* absorption near $n_c/4$ but incorporates thee-dimensional-ray trace, inverse bremsstrahlung absorption, cross-beam energy transfer and nonlocal electron transport.) As seen in Fig. 4 the measured electron temperatures vary depending on the viewing direction; the maxima are higher at the HEX port where mainly six beams interact whereas the observations through a beam port see predominately four-beam interactions. Thus, both the onset of the temperature excursions and the observed maxima depend on the viewing direction leading to the inferred existence of temperature islands over the target surface.

These temperature islands also entail perturbations in the isodensity surfaces near $n_c/4$ of ~ 10 μm due to the isobaric nature of the corona. Similar temperature and density perturbations have been reproduced using the two-dimensional hydrodynamic code DRACO [36] for axisymmetric simulations of a 23° cone section around the axis of symmetry. Up to 30% of the locally incident laser power was artificially deposited within a layer of 50 μm radius (10°cone) $\times$ 10 μm depth at an electron density of $0.237 > n_e/n_e > 0.25$. In contrast, the corresponding observed fraction in energetic electrons [24,37] typically remains at $\lesssim 1\%$. This is consistent with the power deposited by collisional damping of TPD plasma waves that significantly exceeds the energy imparted to energetic electrons [21].

These experiments demonstrate the diagnostic importance of $\omega/2$ spectra. In contrast, $3\omega/2$ spectra are generated by Thomson upscattering and require broad plasma wave spectra. The complex OMEGA beam configuration results in $3\omega/2$ spectra that depend on the illumination pattern on target rendering them of limited diagnostic value. A more quantitative comparison between simulations and observations can be anticipated in the future as nonlinear three-dimensional TPD models [22] are extended to describe half-harmonic emission in detail. Of real importance would be the incorporation of a heuristic TPD model into the hydrodynamic codes, particularly two-dimensional codes like DRACO, as locally varying energy deposition could affect drive energy and implosion symmetry.

In conclusion, spatially and temporally resolved half-harmonic spectra and images of laser-driven implosions show clear evidence for the multibeam nature of the TPD instability, its rapid nonlinear evolution, and its limited spatial extent. The long wavelength TPD (including the absolute TPD instability) produces an identifiable spectral signature that serves as excellent coronal electron temperature diagnostic. The broad spectral features that develop essentially simultaneously across the spectrum are identified as the nonlinear phase of the TPD instability that extends rapidly to the Landau cutoff. Present experimental diagnostics show no evidence for a linear TPD regime. These results are in qualitative agreement with recent TPD simulations. Electron temperature measurements and $\omega/2$ images point toward localized temperature islands near $n_c/4$, where temperatures may exceed the average by 10% to 20% and entail localized density surface perturbations.

This work was supported by the U.S. Department of Energy Office of Inertial Confinement Fusion under Cooperative Agreement No. DE-FC52-08NA28302, the University of Rochester, and the New York State Energy Research and Development Authority. The support of the DOE does not constitute an endorsement by the DOE of the views expressed in this Letter.

*Corresponding author.
seka@lle.rochester.edu

[1] M. V. Goldman, Ann. Phys. (N.Y.) **38**, 95 (1966).
[2] M. V. Goldman, Ann. Phys. (N.Y.) **38**, 117 (1966).
[3] M. N. Rosenbluth, Phys. Rev. Lett. **29**, 565 (1972).
[4] C. S. Liu, M. N. Rosenbluth, and R. B. White, Phys. Rev. Lett. **31**, 697 (1973).
[5] M. N. Rosenbluth, R. B. White, and C. S. Liu, Phys. Rev. Lett. **31**, 1190 (1973).

[6] A. Simon, R. W. Short, E. A. Williams, and T. Dewandre, Phys. Fluids **26**, 3107 (1983).
[7] B. B. Afeyan and E. A. Williams, Phys. Rev. Lett. **75**, 4218 (1995).
[8] J. D. Lindl, *Inertial Confinement Fusion: The Quest for Ignition and Energy Gain Using Indirect Drive* (Springer-Verlag, Berlin, 1998).
[9] D. W. Phillion, E. Campbell, K. Estabrook, G. Phillips, and F. Ze, Phys. Rev. Lett. **49**, 1405 (1982).
[10] W. L. Kruer, *The Physics of Laser-Plasma Interactions, Frontiers in Physics*, Vol. 73, edited by D. Pines (Addison-Wesley, Reading, MA, 1988), p. 96.
[11] W. Seka, D. H. Edgell, J. F. Myatt, A. V. Maximov, R. W. Short, V. N. Goncharov, and H. A. Baldis, Phys. Plasmas **16**, 052701 (2009).
[12] W. Seka, B. B. Afeyan, R. Boni, L. M. Goldman, R. W. Short, K. Tanaka, and T. W. Johnston, Phys. Fluids **28**, 2570 (1985).
[13] D. A. Russell and D. F. DuBois, Phys. Rev. Lett. **86**, 428 (2001).
[14] R. Yan, A. Maximov, C. Ren, and F. Tsung, Phys. Rev. Lett. **103**, 175002 (2009).
[15] R. Yan, A. V. Maximov, and C. Ren, Phys. Plasmas **17**, 052701 (2010).
[16] H. X. Vu, D. F. DuBois, D. A. Russell, and J. F. Myatt, Phys. Plasmas **17**, 072701 (2010).
[17] R. Yan, C. Ren, J. Li, A. V. Maximov, W. B. Mori, Z.-M. Sheng, and F. S. Tsung, Phys. Rev. Lett. **108**, 175002 (2012).
[18] H. X. Vu, D. F. DuBois, J. F. Myatt, and D. A. Russell, Phys. Plasmas **19**, 102703 (2012).
[19] H. X. Vu, D. F. DuBois, D. A. Russell, and J. F. Myatt, Phys. Plasmas **19**, 102708 (2012).
[20] J. F. Myatt, J. Zhang, J. A. Delettrez, A. V. Maximov, R. W. Short, W. Seka, D. H. Edgell, D. F. DuBois, D. A. Russell, and H. X. Vu, Phys. Plasmas **19**, 022707 (2012).
[21] J. F. Myatt, H. X. Vu, D. F. DuBois, D. A. Russell, J. Zhang, R. W. Short, and A. V. Maximov, Phys. Plasmas **20**, 052705 (2013).
[22] J. Zhang *et al.* (to be published).
[23] R. W. Short, J. F. Myatt, and J. Zhang, Bull. Am. Phys. Soc. **58**, 00009 (2013).
[24] R. E. Turner, D. W. Phillion, B. F. Lasinski, and E. M. Campbell, Phys. Fluids **27**, 511 (1984).
[25] R. L. Berger and L. V. Powers, Phys. Fluids **28**, 2895 (1985).
[26] C. Stoeckl *et al.*, Phys. Rev. Lett. **90**, 235002 (2003).
[27] D. T. Michel *et al.*, Phys. Plasmas **20**, 055703 (2013).
[28] D. T. Michel, A. V. Maximov, R. W. Short, S. X. Hu, J. F. Myatt, W. Seka, A. A. Solodov, B. Yaakobi, and D. H. Froula, Phys. Rev. Lett. **109**, 155007 (2012).
[29] T. R. Boehly *et al.*, Opt. Commun. **133**, 495 (1997).
[30] Y. Lin, T. J. Kessler, and G. N. Lawrence, Opt. Lett. **20**, 764 (1995).
[31] S. Skupsky, R. W. Short, T. Kessler, R. S. Craxton, S. Letzring, and J. M. Soures, J. Appl. Phys. **66**, 3456 (1989).
[32] W. R. Donaldson, R. Boni, R. L. Keck, and P. A. Jaanimagi, Rev. Sci. Instrum. **73**, 2606 (2002).
[33] J. Delettrez, R. Epstein, M. C. Richardson, P. A. Jaanimagi, and B. L. Henke, Phys. Rev. A **36**, 3926 (1987).
[34] V. N. Goncharov *et al.*, Phys. Plasmas **15**, 056310 (2008).
[35] I. V. Igumenshchev *et al.*, Phys. Plasmas **19**, 056314 (2012).
[36] P. B. Radha *et al.*, Phys. Plasmas **12**, 056307 (2005).
[37] D. H. Froula *et al.*, Phys. Rev. Lett. **108**, 165003 (2012).